

# **Integrated Interpretation: Using Seismic to De-Risk the Duvernay**

R. M. Weir, D. C. Lawton, and L. R. Lines

## **ABSTRACT**

Development of a resource play such as the Duvernay Formation is subject to intrinsic risks. These may include the risk of incurring additional costs due to an induced seismic event, or risks associated with unexpected thermal maturity, which can determine the value of the processed hydrocarbons (dry gas vs. condensate). These two risks may be related, as the presence of basement faulting may influence the heat flow from the basement, causing local variations in thermal maturity. The presence of basement faulting may also increase the risk associated with induced seismicity, whereby pre-existing faults are reactivated during the course of well treatment. Interpretation is complicated by the variable depositional environment for the Duvernay marine shale; an off-reef depositional system includes mechanisms such as contourite deposition, turbidity/mass flow, and in-situ biological carbonate precipitation, thereby creating variances in total organic hydrocarbon content. Transtensional faulting caused by deep seated strike-slip faults may be reactivated during a completion program, rather than induced hydraulic fractures. Combining the microseismic and reflection data and displaying the data in depth allows the joint interpretation of reflection seismic and microseismic data. A geological picture is constructed by visualizing microseismic hypocenters in a chair plot with reflection surfaces and depth slices. These can be used to determine best practices for the future location and design of horizontal treatment wells.

## **INTRODUCTION**

The Duvernay Formation is an unconventional hydrocarbon play in Western Canada and is the object of active horizontal development drilling using hydraulic-fracture stimulation. The Fox Creek area is located in the center of a major resource play within the Duvernay Formation (Preston et al., 2016) (Figure 1). The map displays regional thermal maturity in the region, highlighting the areas prone to gas, condensate, and oil recovery within the Duvernay formation. Our specific study areas near the town of Fox Creek are covered by two 3-D/3-C seismic surveys, and are named ToC2ME and Bigstone North, respectively. These study areas are contained within the larger condensate (or natural gas liquids, NGL) prone area, which is the desired target for economic development in this region, and is shown by the yellow band in Figure 1. The Duvernay oil region is mapped to the northeast with the dry gas region to the southwest of Fox Creek.

## **GEOLOGY**

The formation of interest is the Devonian age Duvernay Formation, which is overlain by the Ireton Formation shale, and sits conformably on the Swan Hills Formation (Switzer et al., 1994). Figure 2 shows the associated stratigraphic table with the schematic cross section. The Duvernay Formation is an organic rich calcareous shale (Knapp et al., 2017), deposited contemporaneously with the Leduc Formation reef complex. In this marine envi-

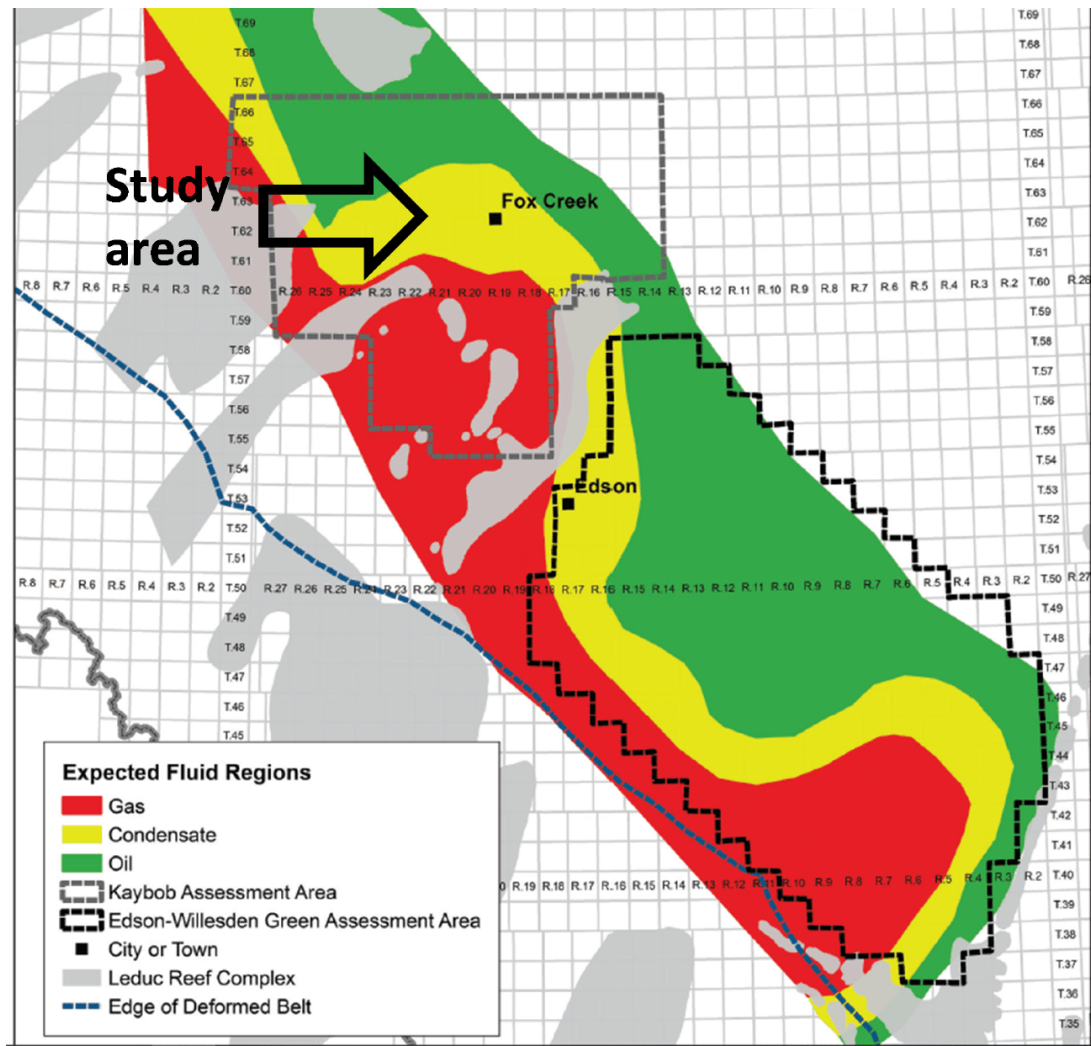


FIG. 1. Expected fluid regions within the Duvernay play, given the thermal maturity profiles (modified from Preston et al. (2016)). In the regional context, our study area is situated within the condensate fluid region, highlighted with the arrow.

ronment, three mechanisms of deposition of the Duvernay were recognized by Knapp et al. (2017); marine snow (in-situ carbonate distribution caused by biological activity), gravity flow (turbidity deposits from the reef and reef edge), and contourite deposition (caused by marine currents running parallel to the existing reef fronts and shelf breaks). The Duvernay was classified by Knapp et al. (2017) in terms of ten geological facies, varying in lithology, organic content, and bioturbation. The deposits making up the Duvernay Formation were rich in organic matter, and deposited in an oxygen deprived environment. After burial and heating, the rich organic matter generated hydrocarbons by the processes of catagenesis and metagenesis (Tissot and Welte, 1984).

Petroleum generation in the Duvernay Formation was a function of organic content, temperature, pressure, and time (Tissot and Welte, 1984). Kerogen (solid, insoluble organic matter) was changed to oil, gas and condensate by a process called catagenesis. The first stage of catagenesis was the formation of oil, generating hydrocarbons with a medium to low molecular weight. With pressure (burial) and a temperature increase, carbon-carbon

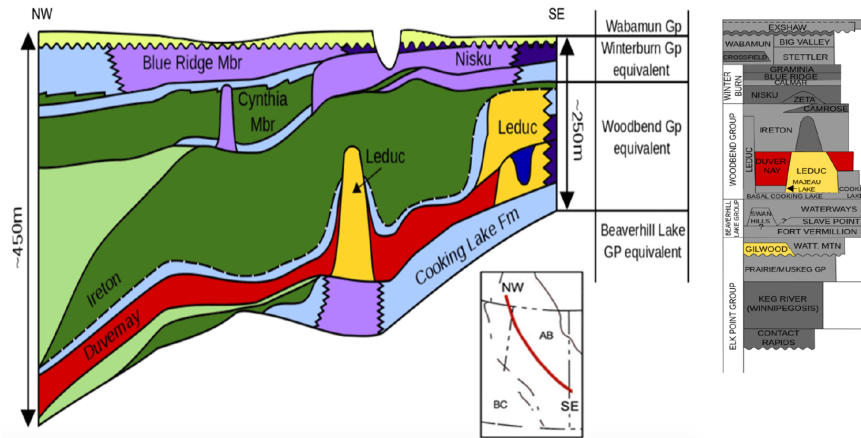


FIG. 2. A schematic cross section showing the Duvernay Formation with its geological setting, modified from Preston et al. (2016). The Duvernay Formation (highlighted in red) is the stratigraphic equivalent of the Leduc Formation, and is the focus of this study.

bonds continued to break, creating the wet gas condition. In the final stage, called meta-genesis, most of the available organic matter had previously been consumed through cata-genesis. Large amounts of methane were generated from the cracking of the source rock hydrocarbon and the liquid petroleum reservoir. The methane in the rock was quite stable, and was not readily destroyed by high temperatures. Tissot and Welte (1984) state that methane will remain stable up to temperatures as high as 550°C.

Preston et al. (2016) placed the general Fox Creek area within the Condensate (NGL) region for the Duvernay Formation (Figure 1). Figure 3 is a smaller area (within the larger condensate region) that encompasses both the seismic reflection and microseismic surveys. The cumulative production data from the Duvernay are displayed as pie charts, with the size of the circle proportional to the cumulative production. Red refers to condensate, blue is water, yellow is gas, and green refers to oil. The small green crosses displayed show the epicenters of recorded seismicity associated with hydraulic fracturing. Although the area displayed in Figure 3 is within the regional condensate window, the production displayed on the map shows reported volumes of dry gas, condensate, and gas plus condensate production. Some of the wells also have significant reported water volumes. Condensate volumes are often under-reported, as reporting requirements require natural gas liquids (NGL/Condensate) to be either reported as gas or oil (AER directive 017 13.2.2). It is up to the operator to report condensate (NGL) volumes on a voluntary basis.

A regional study in the Fox Creek area (Shen et al., 2019) demonstrated that the maximum horizontal stress axis is  $\sim 43^\circ$  from north within the Duvernay Formation. This study was 150 by 150 km, and encompasses both the Bigstone North and ToC2ME areas (the area enclosed in Figure 3). The map area displayed in Figure 2 is contained within the larger regional study published by Shen et al. (2019). Horizontal wellbore placement in the study area is generally based on the assumption that induced fractures propagate in the direction of  $S_{Hmax}$ . The assumption made in drill planning is that an orientation orthogonal to  $S_{Hmax}$  will allow hydraulic fractures to propagate at a right angle, maximizing the stim-

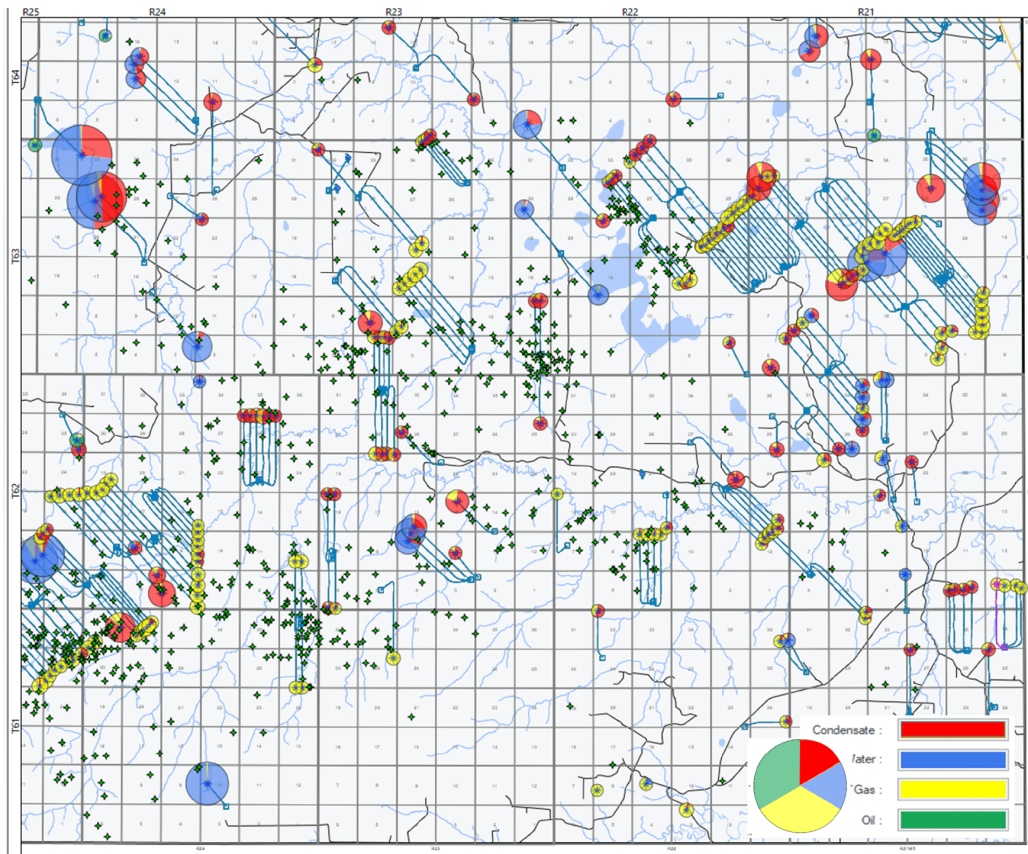


FIG. 3. A regional map showing the wells that have been completed in the Duvernay formation (green lines). The pie chart represents the type of production; red is condensate, yellow is gas, and blue is water. According to the reported data, there is no oil production in this map area (green). Most of the Duvernay wells have been drilled in a NW-SE orientation, perpendicular to  $S_{Hmax}$ . The reporting of condensate production is not a requirement, therefore condensate volumes tend to be under-reported (AER Directive 017 13.2.2). Sizes of the pie charts are proportional to the quantity of production to-date (October 2019). Induced seismic event locations are shown as green stars (<https://www.inducedseismicity.ca/catalogues/>).

ulated reservoir volume (Eaton, 2018). As can be seen, many of the well locations shown on the map are positioned to be oriented orthogonal to  $S_{Hmax}$ ; however, some of the wells are oriented north-south due to land ownership constraints.

## REFLECTION SEISMIC DATA

Two seismic volumes are used in this study which are referred to here as ToC2ME and Bigstone North. These are located in adjoining areas and have a small overlap. Detailed structural maps were constructed using geological ties as defined by the synthetic seismogram in Figure 4. This seismogram was also used to determine the time-to-depth relationship and depth convert the seismic volumes. Depth and time scales are shown on the synthetic with the sonic and density curves. The first step in the interpretation process is to correlate the seismic data to the geological column. Here, a synthetic seismogram (blue traces, Figure 4) is created from a sonic and density log by creating an acoustic impedance series. This acoustic impedance log is in turn convolved with a wavelet and generates the synthetic seismogram (the blue curve in Figure 4). By matching the synthetic seismogram

to the actual reflection data (red), reflection horizons are correlated to the well log depths. This correlation establishes the time depth relationship in the P-P domain and correlates the seismic reflection markers to geological horizons. The target zone, the Duvernay Formation, is highlighted with an arrow, as is the underlying Swan Hills Formation. The full interpretation and inversion workflows used for this data are described in Weir et al. (2018) and Weir et al. (2019), respectively.

The structural interpretation incorporated structural geology concepts such as strike-slip faulting, flower structures, and transcurrent faulting. The technique used for fault interpretation was observing matching vertical displacements in reflection horizons and interpolating vertically between them. Within these seismic volumes channel structures could be observed within the Gilwood Formation (within the deeper Elk Point Group as well as a major Swan Hills reef front (Switzer et al., 1994)). The Gilwood channel is interpreted to have significant lateral displacement in the seismic volume, as does the Swan Hills reef front. These lateral displacements are herein interpreted as strike-slip faults in the seismic volume. In some instances, there appear to be minimal vertical displacements on the same faults.

### **MICROSEISMIC DATA**

The microseismic hypocenters for the ToC2ME portion of this study were processed by using the “Focal Time Method” as described by Poulin et al. (2019) (Figure 8). This method was used to convert the microseismic event time picks to depth. For the Bigstone North area, hypocenters were determined as described in Eyre et al. (2019b). Loading these hypocenter locations into the seismic workstation provided an independent set of data to be used in the seismic interpretation. For the Bigstone North area, the microseismic hypocenters delineated predominantly north-south aligned structures (Eyre et al., 2019b). In the ToC2ME data, the hypocenters formed two distinct alignments; N-S aligned structures in the Upper Ireton Formation carbonate, and a 30° from north alignment in the Duvernay Formation treatment interval (Eaton et al., 2018). How these alignments are factored into the interpretation will be discussed later in this paper.

For the ToC2ME area, moment tensor inversion provided information as to the nature of the fracture or fault deformation of the seismic event clusters (Zhang et al., 2019), displayed in the form of beach ball diagrams. Figure 7 illustrates the source mechanisms of two groups of microseismic data; in this area the source mechanisms were seen to be primarily strike-slip faults. Figure 7 also shows a map of 4,108 epicenters of the induced events, as well as the locations of the treatment wells. The beach ball diagrams are shown for clusters 4 and 5; cluster 4 indicates a N-S strike-slip motion, which is later used in the fault interpretation. Similar source mechanisms were found by Eyre et al. (2019b) for the Bigstone North area. The largest induced event that was recorded during the ToC2ME treatment program was  $M_w$  3.2, which triggered shallower events in cluster 4. The hypocenters for cluster 4 are approximately 70 meters above the Duvernay Formation treatment interval (Figure 8) (Poulin et al., 2019).

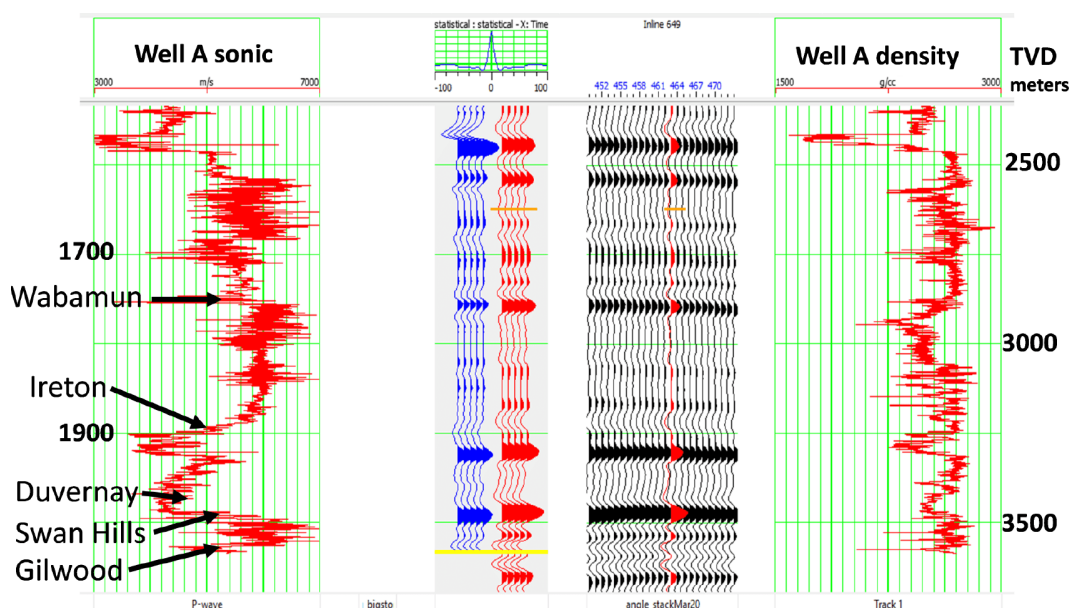


FIG. 4. PP synthetic well tie. Sonic and density well logs are shown, as well as the synthetic seismogram (blue) and actual reflection data (red, black). The synthetic seismogram tie shows the correlation of the key seismic horizons, as well as the corresponding depths. The treatment zone is the Duvernay Formation of the Upper Devonian, shown on the well tie. The match between the blue and red traces shows the final correlation.

## REFLECTION DATA AND MICROSEISMIC JOINT INTERPRETATION

The seismic interpretation process used here used a synthetic generation, horizon correlation and depth conversion. This was followed by a manual fault identification using matching vertical displacements of reflectors, and lateral offsets of geological features. A fault detection volume was used in conjunction with the conventional reflectivity seismic volume. The microseismic hypocenters were used as an independent point set to be used in the interpretation process.

Time structure maps were generated based on the synthetic seismic traces correlated to the PP reflection data. For the ToC2ME seismic volume, the top Devonian (Figure 5(a)) (Wabamun Group), and Top Swan Hills (Figure 5(b)) are shown. The position of well “A” (well data used to construct the synthetic seismogram) is shown in both volumes, with the color bar corresponding to isochron values. With this display the Swan Hills surface shows two distinct structural lineations; one is approximately north-south, while the other is north-northeast to south-southwest. The Wabamun time surface is structurally high to the east, with N-S trends, some of which correspond to features in the Swan Hills time surface.

Due to the orientations of lineations in the volume and the strike-slip source mechanisms of induced seismicity in the region (Zhang et al., 2019), the fault system is interpreted to be a flower structure (Figure 6), a result of deep seated strike-slip movement and the resulting displacements in the shallower mid to upper Devonian horizons. This matches the findings of other studies in the region (Zhang et al., 2019; Eyre et al., 2019b; Wang et al., 2017). The structural lineation is primarily north-south, with minor vertical displacement.

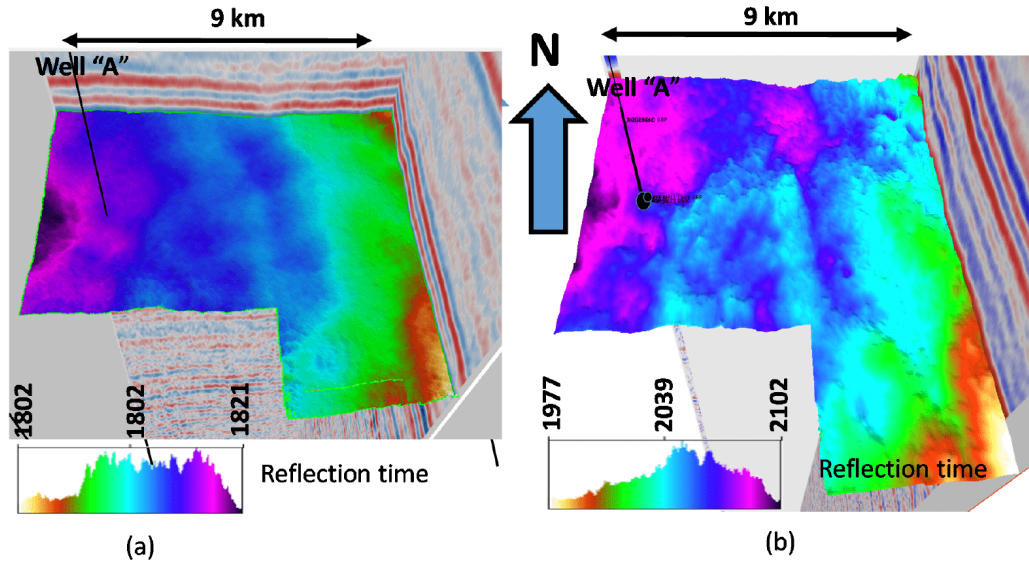


FIG. 5. 3D views of seismic data near the ToC2ME program. (a) Wabamun and (b) Swan Hills time structure maps. The treatment zone, the Duvernay, sits conformably above the Swan Hills Formation. The color bar is in subsea depth (m).

Transcurrent faulting, also referred to as transpression and transtension, forms within deformation zones that deviate from the major strike slip faults (Fossen and Tikoff, 1998). These faults form complex fault systems, running oblique to the main strike-slip motion. Transcurrent faulting can occur when there is a deviation in the linear strike-slip fault in direction, or as the net displacement of the larger fault system moves laterally from one strike-slip fault to the next (Figure 6(a)). On a local scale, if the adjoining strike-slip faults are converging, a transpressional system results; if they diverge a transtensional system results. The small structural patterns on the Swan Hills surface occurring between the major strike slip faults are interpreted to be transtensional faults, later described in the “Interpretation and Analysis” section of this paper.

Figure 7 is a map view display of the ToC2ME seismic event catalogue. The microseismic hypocenters are labeled as clusters 1 through 6. The color bar used is in terms of time, displaying events from October to November. Cluster 4 has a calculated hypocenter depth that is centered in the Upper Ireton carbonate, 70 meters above the Duvernay treatment zone (Figure 8). It includes the largest induced seismic event caused by the HF treatment ( $M_w$  3.2), and the associated aftershocks. The beachball diagram shows the calculated average focal mechanism for these events, indicating a N-S strike-slip motion. For clusters 1, 2, 3, 5, and 6 the seismic events are centered on the Duvernay treatment interval. For these clusters, the direction of induced fracture propagation is around  $30^\circ$  from north. In contrast, the published  $S_{Hmax}$  is shown on the lower right hand corner of Figure 7, with a direction of  $43^\circ$  from north (Shen et al., 2019).

Combining the microseismic hypocenters with the depth-converted seismic volume results in the chair display shown in Figure 9. From the focal time event catalog, 13,105 hypocenters were loaded along with the depth converted seismic P-P volume into the inter-

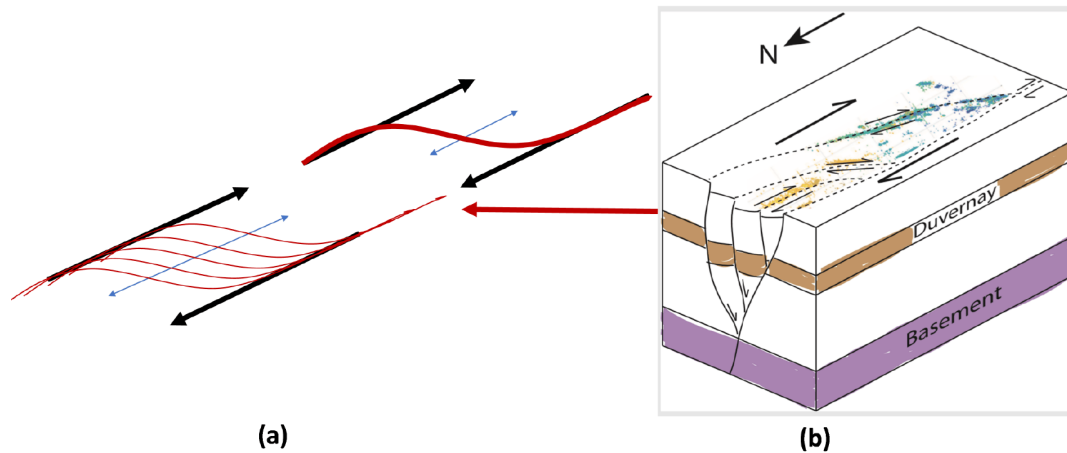


FIG. 6. (a) Schematic diagram of a transtensional fault system in the Duvernay. The movement of the strike-slip fault is transferred to a number of cross-cutting faults. (b) Schematic diagram of a Precambrian fault, and the associated flower structure (Eyre et al., 2019b). According to this model, the flower structure extends from the basement into the sedimentary section. This diagram represents the structural interpretation of the Duvernay Formation using the seismic data in this report (Weir et al., 2018).

pretation software. The directional surveys from the horizontal wellbores were also loaded into the interpretation software, as well as the seismic “Fault Detect” volume previously constructed. The displayed 3-D volume is a co-rendered structural stack combined with an edge-detect volume. The depth slice intersects an interpreted Gilwood channel system, which is seen to meander through the seismic volume from left to right. There is an observable displacement from north to south along the interpreted strike-slip fault. Cluster 4 of the microseismic data appears to align with this fault, situated nearly directly above the strike-slip displacement in the Gilwood Member.

The large lateral ( $\sim 2$  km) displacement observed on the Gilwood channel was correlated with fault interpretation lines, and a lineation of induced events (cluster 4) was correlated spatially with the fault interpretation lines in the same manner. This proved to be particularly useful, in that the fault associated with cluster 4 had very little vertical displacement, but had a clearly defined linear alignment. Interpolating a fault plane between the user-defined interpretation lines gives a 3D fault volume using both reflection and microseismic data. The N-S movement of this fault is independently confirmed by observing the beach ball plot associated with cluster 4 (Figure 7) (Zhang et al., 2019).

The Swan Hills formation is a strong seismic reflector directly below the Duvernay Formation. Given that there is not a strong reflection event associated with the Duvernay Formation, the Swan Hills serves as an excellent proxy for the Duvernay structure (Weir et al., 2019). The Swan Hills structure is presented in Figure 10 as a red to blue map, calibrated in depth, and viewed from the north. There are observable structural lineations in the Swan Hills surface, oriented  $30^\circ$  from north in the vicinity of the wellbores. Figure

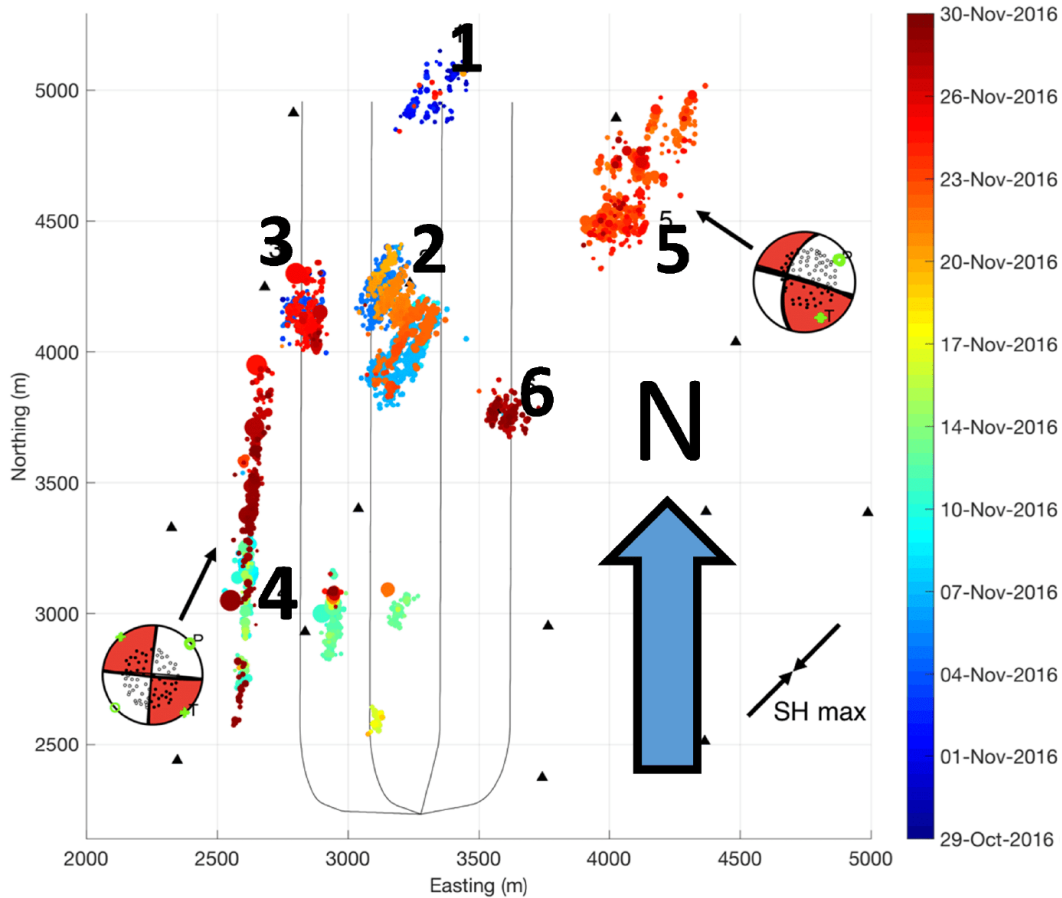


FIG. 7. Epicenter locations of induced events with two examples of focal mechanisms (modified from Eaton et al. (2018)). Group 4 is a  $M_w$  3.2 induced seismic event followed by aftershocks occurring in the upper Ireton Formation, approximately 70 meters above the treatment zone. It shows a N-S lineation, with a strike-slip mechanism derived from moment tensor inversion. The principle stress axis is plotted. Cluster 5 shows a predominantly strike-slip motion with a NNE-SSW orientation and a small vertical component.

10(b) shows the alignment of the induced events with the major Swan Hills structural alignments. However, more minor pre-existing structures can also be observed as indicated with the arrows in Figure 10(a), and also appear to align with many of the lineaments observed in the microseismic data. These are not aligned with the  $S_Hmax$  direction, which is also indicated.

## DISCUSSION

Previous work on the 3D seismic volume in the ToC2ME area (Weir et al., 2018) details significant structural and compositional variations within the Duvernay Formation. Inversion-derived stratal slices show lateral impedance variations within the Duvernay Formation. Joint inversion produced maps of the Poisson's Ratio, Young's Modulus, and brittleness index, indicating that faulting had a significant effect on rock properties. Detailed examination of the Swan Hills depth-structure map shows a dominant trend of NNE to SSW structural lineations (Cluster 2), abruptly terminating against a major N-S fault to the

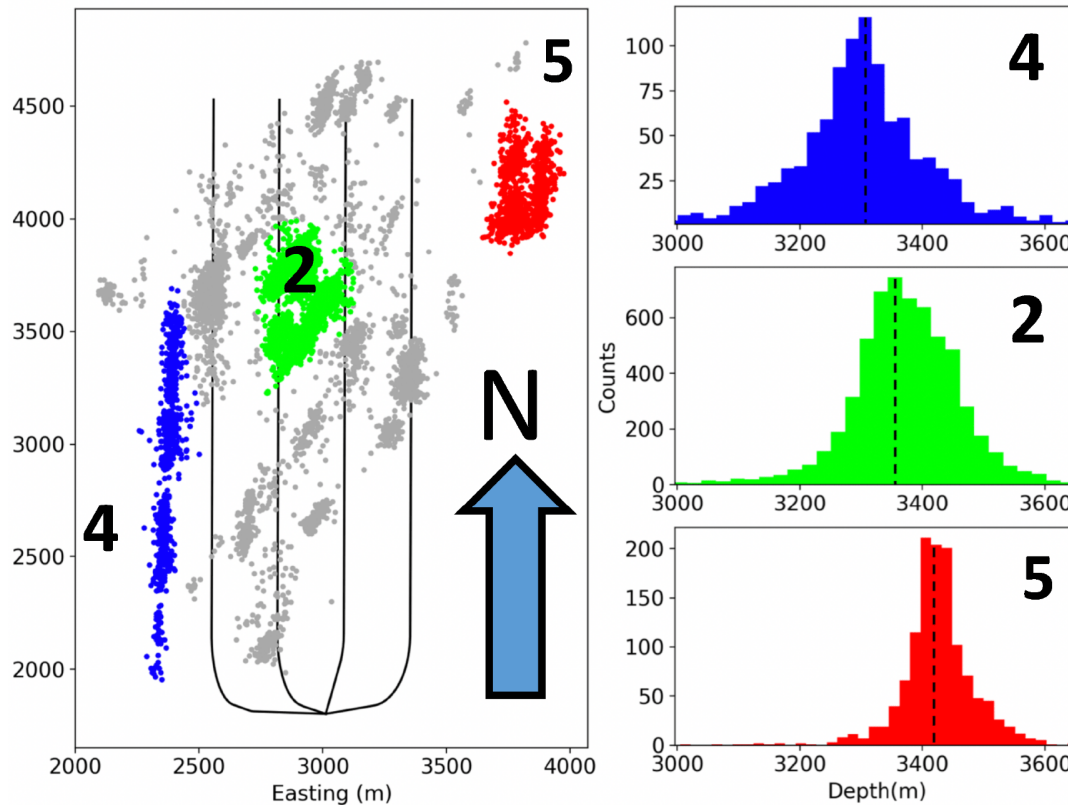


FIG. 8. Depth histograms of the calculated hypocenters for three of the microseismic clusters and map of those clusters (from Poulin et al. (2019)). The blue cluster (4) is centered at 3300 meters, the green and grey (2) at 3370 meters, and the red (5) at 3425 meters. The blue events in cluster 4 are associated with the largest induced earthquake.

East (Cluster 5) (Figure 10). The abrupt termination of cluster 5 against a deep-seated fault appears to confirm the hypothesis that rock properties may play a major role in fracturing. Also noteworthy is that the pattern of microseismic activity observed in cluster 2 follows the same NNE-SSW alignment as can be observed in the present-day Swan Hills structure. This suggests that what is being observed in the microseismic catalogue is the re-activation of pre-existing faults, and not hydraulic fractures.

Interpreting the Swan Hills Formation lineations in terms of transtensional faulting explains the predominant  $30^\circ$  direction between the bounding N-S strike-slip faults. The faulting on the Swan Hills Formation is predominantly  $30^\circ$ , in the vicinity of the treatment wells, but this varies throughout the 3-D depth structure. Above the Swan Hills sits the Duvernay and Ireton formations. The transtensional faulting may terminate within the shales of the Ireton Formation; these shales tend to deform in a ductile manner, rather than via faulting or fracturing (Eyre et al., 2019a). This is a possible explanation as to why the transcurrent faulting is not observed in the Upper Ireton Carbonate, or the Upper Devonian Winterburn Group.

In the same manner, the large displacement N-S fault aligns with the major induced seismic events (cluster 4), observed 70 meters above the treatment zone. Eyre et al. (2019a) proposed that the triggering mechanism for the large induced seismic event was caused

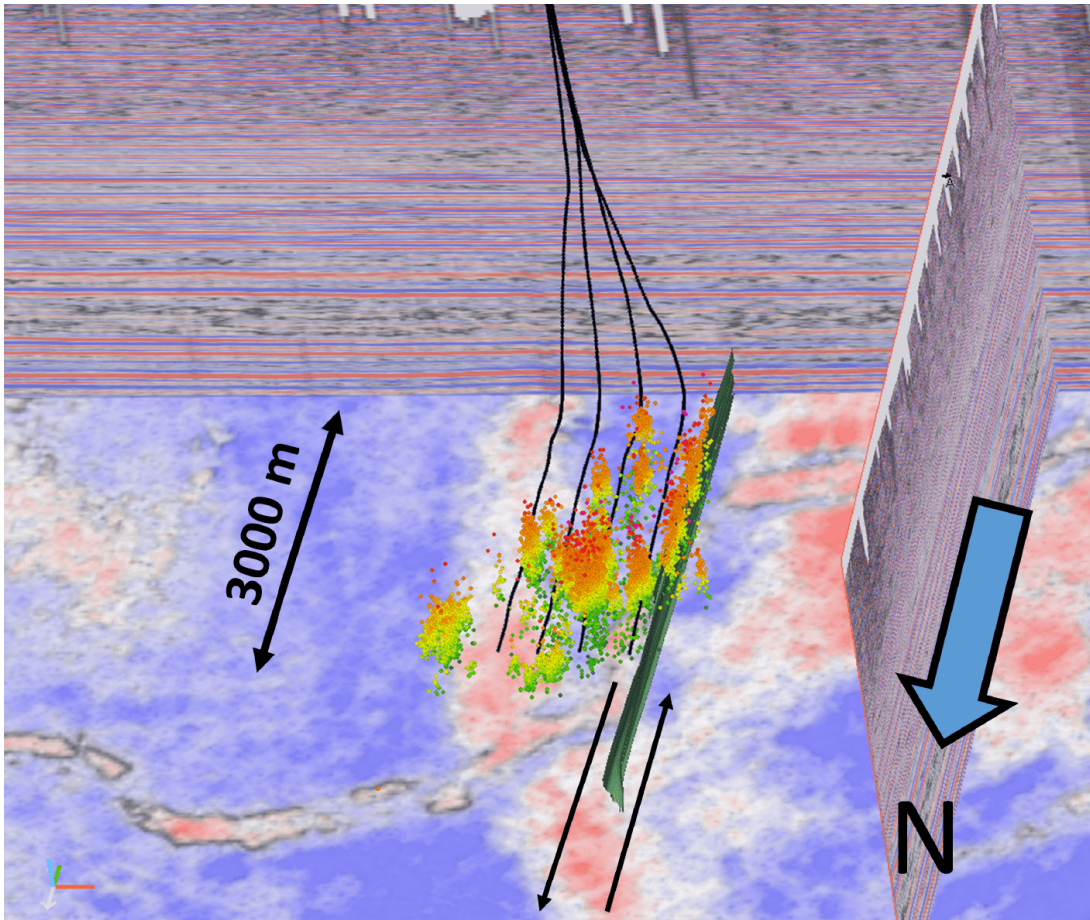


FIG. 9. Gilwood time slice (viewed from north), a co-rendered fault detect volume with amplitude (red to blue). The Gilwood channel-like feature appears to be displaced approximately 3000 m across the interpreted left lateral fault. The microseismic events from cluster 4 are observed to occur approximately 300 m directly above this fault.

by aseismic creep of the Duvernay/Ireton Formation along a pre-existing N-S deep-seated fault, that was initiated by pore pressure increase due to the fluid injection. The alignment between the deep-seated fault in the Gilwood Formation and the induced seismicity (Cluster 4) confirms that a deep-seated fault was reactivated during the course of hydraulic fracture treatment of the Duvernay formation, with events occurring significantly above the reservoir, as observed by Eyre et al. (2019b). The N-S event cluster appears to be at the depth of the Upper Ireton Carbonate.

The area Bigstone North incorporates the northern portion of the 3-D/3-C seismic reflection survey. It serves as a second case study to examine the relationship between geological structure and microseismic event propagation. This area is covered with the 3-D/3-C seismic data volume, co-located with a passive microseismic array. As in the ToC2ME data, this area has microseismic events and induced seismicity with aftershocks triggered by the hydraulic well treatment program.

Previous work on this data (Weir et al., 2019) shows the results of structural interpretation and joint inversion. This work again demonstrates that there are significant variations

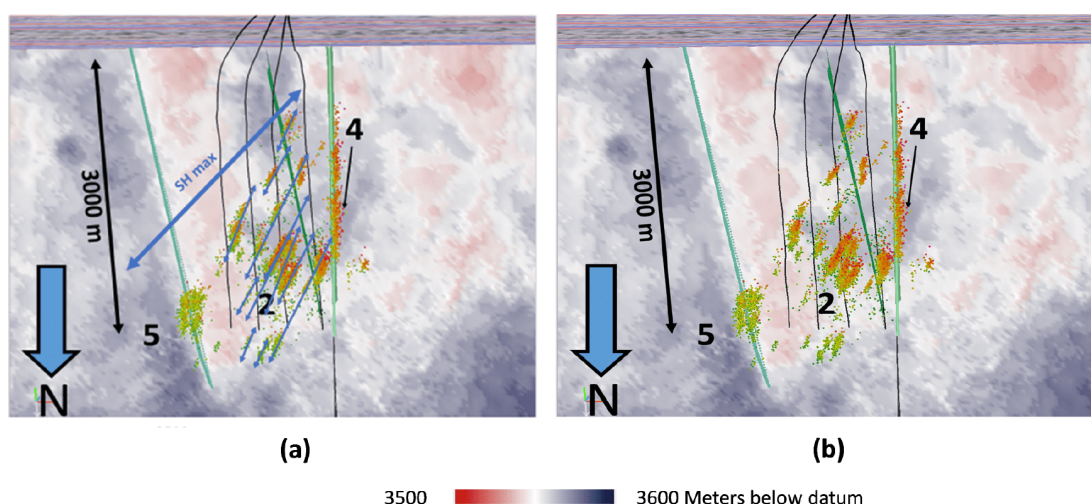


FIG. 10. Swan Hills Formation depth-converted structure, viewed from north. Cluster 2 occurs at the Duvernay Formation treatment depth. There is a pronounced NNE-SSW structural trend on the underlying Swan Hills Formation (SWH), which matches the orientation of cluster 2 events from the microseismic data (a). Since the Duvernay conformably overlies the SWH, this map also approximates the Duvernay depth structure. Cluster 5, occurring at the treatment depth, terminates abruptly in the northeast against an interpreted vertical fault that does not appear to activate (b). Cluster 4 appears to align with the main fault that was activated by this treatment, which is oriented N-S (b). The structural lineaments that are aligned  $30^\circ$  from north are consistent with the interpretation of transtensional tectonics, where strike-slip motion is transferred from one fault to another by a series of intermediate faults.

in Young's modulus, Poisson's ratio and brittleness across the area. These variations may be attributed to the local depositional environment, or post-depositional alteration caused by faulting (geology section).

The structural lineations on the Swan Hills Formation depth map are predominantly N-S, with a notable absence of observable oblique faulting. An explanation for this is that in this local area the basement faulting displacement is predominantly strike-slip, with no convergence or divergence to create transtensional faults. The implication of this is that the fault reactivation, occurring as a result of a fracture stimulation, would occur in a N-S direction, along the path of the pre-existing strike-slip faults.

Figure 11 is an E-W seismic cross-section of the seismic volume. The key elements of this seismic section are the Gilwood channel, the Swan Hills reef edge, and the interpreted near-vertical faults. The Duvernay Formation sits directly above the Swan Hills reflector. The Swan Hills, Gilwood, and Precambrian horizons are shown in depth; these same horizons are displayed in north view map displays in Figures 12-14. The seismic line displayed in Figure 11 is shown as the cross-section A - A' in the map views in Figure 12. The projected depth of the  $M_w$  4.1 seismic event is shown as the yellow star, and is again located significantly above the reservoir within the Wabamun carbonate formation (Eyre et al., 2019a).

Figure 12 displays the depth-converted seismic surfaces on the Swan Hill Formation (a), and the Precambrian basement (b). Figure 13 is a display of the Swan Hills Formation surface. This chair plot viewed from the north highlights both the N-S faulting and the reef

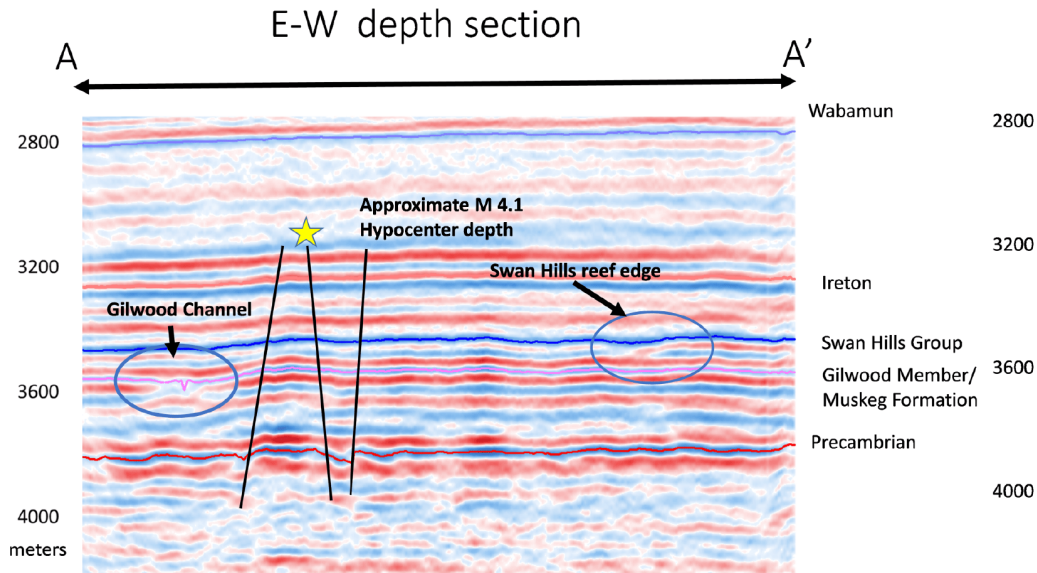


FIG. 11. An east to west depth cross section (modified from Eyre et al. (2019a)) showing the key features in the Bigstone North region. The Swan Hills reef edge, a Gilwood channel, and the vertical displacement associated with the basement strike-slip faults are highlighted. The Swan Hills Group, Gilwood Member, and Precambrian markers are displayed in depth. The projection of the  $M_w$  4.1 seismic event is shown as the yellow star. Associated maps and the interpretation of these features are displayed in Figures 12-14

edge. The Swan Hills Reef is a prominent NE-SW feature displayed in Figure 13(a), shown with a blue outline in Figure 13(b). Notable N-S displacements can be observed along this reef-front. A series of N-S faults are also seen on both the Swan Hills and Precambrian maps; several of these were interpreted and are shown in Figure 13(b). Although these faults are predominantly strike-slip, in some instances, there is noticeable vertical displacement. The faulting is almost entirely N-S, in contrast with the ToC2ME area, where there is a significant NNE to SSW component to the faulting.  $S_{Hmax}$  is displayed as a blue arrow, again  $43^\circ$  from north.

Figure 14 is a depth map of the Gilwood Member/Muskeg formation of the Middle Devonian. The Gilwood Member is a channel that was active during the uplift of the Peace River arch (Switzer et al., 1994). There is a distinct channel-like feature approximately 400 m wide meandering through the map area, changing direction abruptly as it crosses interpreted strike-slip faults. This matches significant displacement in the higher Swan Hills reef front (Figure 13), presumably caused by post-depositional fault movement.

The microseismic events plotted in Figures 12-13 are color-coded with depth. The catalogue is comprised of  $> 10,000$  seismic events, many of which locate above the Duvernay reservoir, and including the  $M_w$  4.1 earthquake with its associated aftershocks. This is the same induced event that Eyre et al. (2019a) used to propose the mechanism whereby aseismic creep can produce an earthquake at a depth shallower than the treatment formation. The microseismicity shows a distinct N-S trend, aligned to the N-S structural lineaments observed on the depth-converted Swan Hills map, as well as the Gilwood map. The Swan Hills reef also appears to present a barrier to hydraulic fracture propagation, as where events

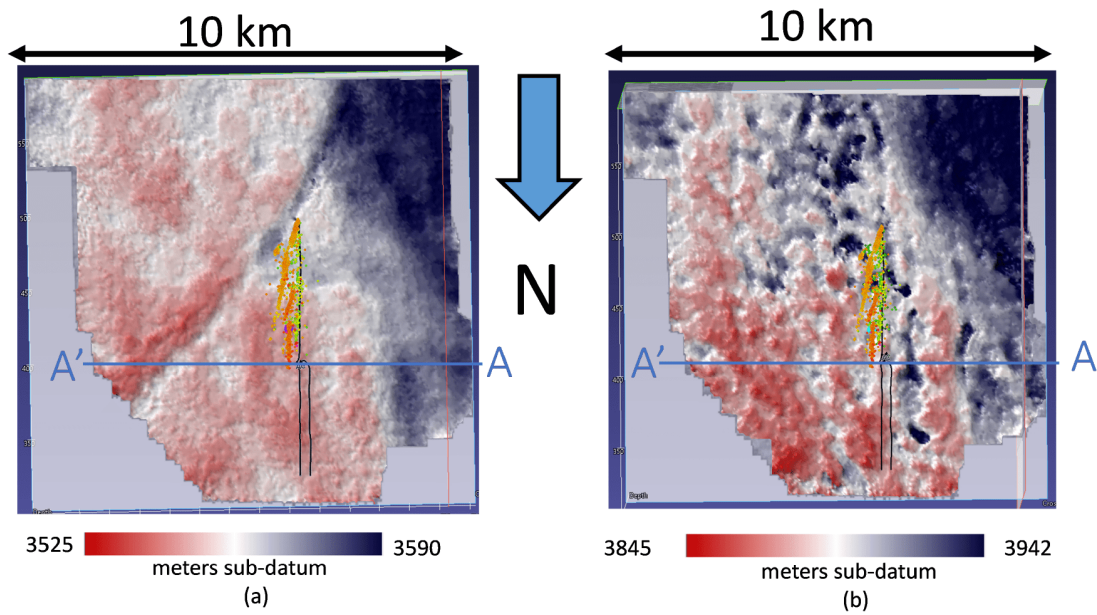


FIG. 12. Map views of depth converted structures for the Swan Hills Formation (a) and Precambrian basement (b). The microseismic catalogue locations are displayed on top of the structure map, showing a distinct north to south alignment, parallel to the observed N-S fault lineaments. The Swan Hills reef front, seen as a NE-SW curved line on the Swan Hills surface (a), appears to have acted as a barrier, inhibiting microseismic growth to the south and east of the treatment well.

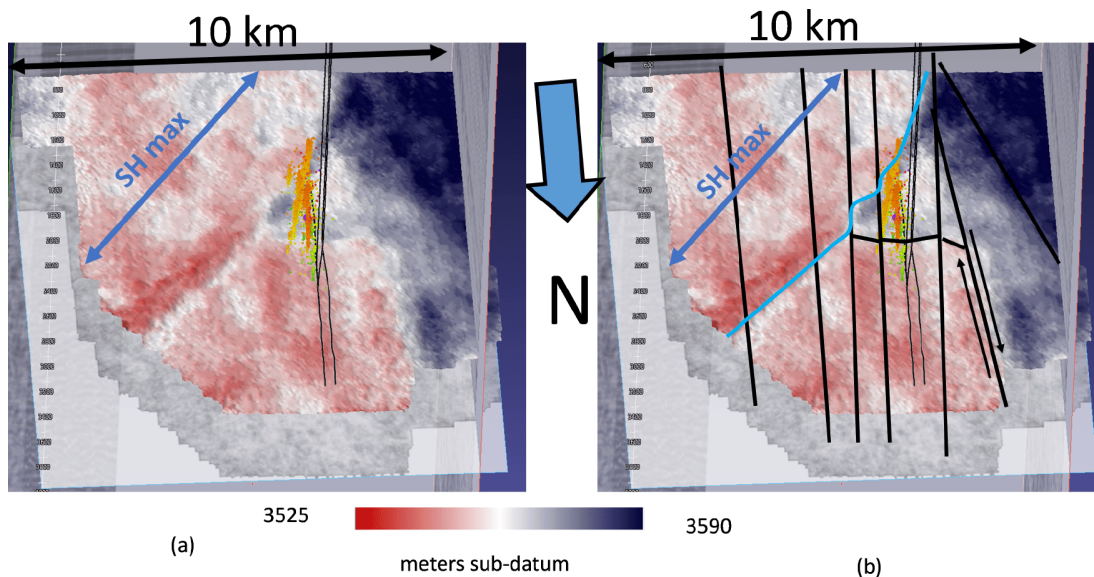


FIG. 13. (a) North view perspective chair plot of the Swan Hills Formation structure, and (b) the interpreted version of the same map. The Swan Hills reef front is blue and deep-seated Precambrian faults are black lines. The microseismic events are shown colored by their corresponding depths.

come close to the reef front, their orientations rotate to reef-parallel. The significant  $M_w$  4.1 event and its aftershocks follow a N-S lineation aligned with a fault mapped to the deep Precambrian (Eyre et al., 2019a).

Fault systems play an important role in fluid flow and advective heat transport in sedimentary basins (Bjørlykke, 2018). Given sufficient upward fluid flux within basement-

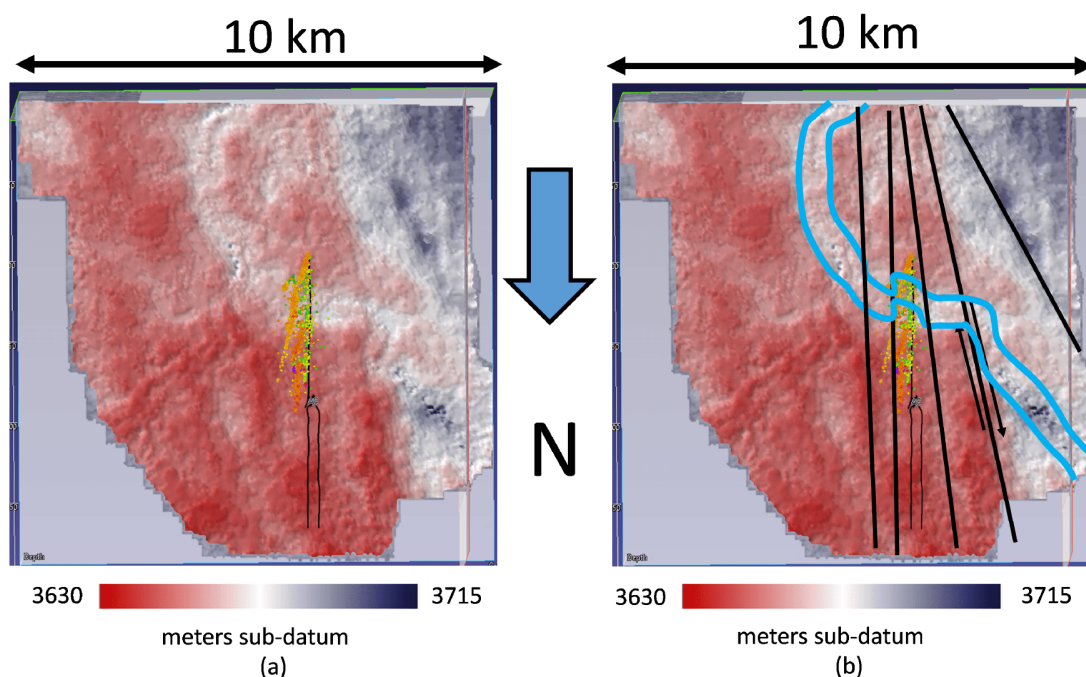


FIG. 14. North perspective view plot of the Muskeg Formation, Gilwood Member. (a) Time structure, and (b) three of the interpreted strike-slip faults with the Gilwood channel highlighted in blue. The microseismic events are shown as points, colored by their corresponding depths.

rooted fault systems, large thermal anomalies can be created (Bjørlykke, 2018). Indeed, the effects of basement-derived fluids in the nearby Simonette oil field (Swan Hills) have been well documented with respect to dolomitization (Duggan et al., 2001). Geochemical data indicate the occurrence of both early and late-stage dolomitization; in the latter case, the fluids are considered to be hydrothermal and basement-sourced along near-vertical faults (Duggan et al., 2001). Further evidence in the WCSB is provided by regional deep-crustal 2D seismic data, which suggest that deep-seated faults could have controlled the fluid-circulation patterns in the basin as well as the orientation of reef foundation during the Devonian (Eaton et al., 1995). Controls on fluid circulation and advective heat transport within sedimentary basins are also well documented for certain types of ore deposits, such as unconformity-related uranium deposits (Li et al., 2016). In this case, basement faults can localize fluid ingress and egress into the sedimentary units and thus establish stable patterns of convective circulation (Li et al., 2016). Thus, the observed basement-seated faulting is likely to play a key role in the thermal maturity of the Duvernay Formation.

### INTERPRETATION AND ANALYSIS

In order to understand the complexities associated with the development of the Duvernay formation, one must address several aspects of the present day Duvernay Formation:

- The organic rich shale was deposited as a result of organic in-situ precipitation, gravity flows, and contourite currents. Pre-existing structures such as the Swan Hills reef front, faulted structure present during deposition, and the Leduc reef complex, are important factors influencing reservoir quality. Joint inversion may address this issue

by displaying reservoir properties (such as brittleness) over the seismic volume.

- Thermal maturity may be affected on a local level by basement faults. The faulting may increase heat flow, and in turn thermal maturity. The Fox Creek area, regionally mapped as condensate-prone, may have localized areas of dry gas due to high heat flow caused by basement faulting. Given the relatively small areas (in a regional sense) of the 3D/3-C seismic surveys, there is not enough data to fully test this hypothesis. Nevertheless, given the local variations observed in Figure 3 in gas, condensate and water production and the observations of basement-seated faults, local variations in heat flow by basement faulting present a plausible explanation for the production.
- Pre-existing faulting and fracturing caused by transtensional tectonics appear to be a significant factor controlling fracture propagation. These structures, created by a releasing step-over within a flower structure, appear to control the direction of induced fracture propagation. We have shown here that these features can be mapped using 3D seismic, and should be considered when planning a horizontal well treatment program. The alignment of microseismic events with transtensional faults indicates that they are the result of the reactivation of existing faults, rather than induced fractures oriented to  $S_{Hmax}$ .
- Strike-slip faults in the region may be critically stressed, and wellbores running in close proximity and parallel to a fault such as this may trigger an induced seismic event of significant magnitude. Aseismic slip in the Duvernay formation caused by hydraulic fracturing may cause induced seismic events in deeper or shallower formations (Eyre et al., 2019a).

The pattern of induced fractures observed in Bigstone North terminates against the underlying reef front (Figure 13). Two possible explanations for this are (i) the reef front itself is a mechanical barrier preventing fracture propagation, or (ii) the facies of the Duvernay varies across the reef front due to the differences in water depth due to deposition. In either case, the fracture stimulation did not propagate across the reef front, leaving the hydrocarbon reserves to the south untouched. A similar pattern is observed for cluster 5 in the ToC2ME region.

## CONCLUSIONS

The results presented here indicate the dominant factor in the propagation of induced seismicity is pre-existing faults within the Duvernay Formation. The ToC2ME data show an alignment of microseismic events with pre-existing Swan Hills structures, as opposed to  $S_{Hmax}$  (Figure 10). In both Bigstone North and ToC2ME areas, the pattern observed for the minor faulting is consistent with transtensional-related strike-slip faulting. Many of these faults can be mapped in the seismic volume from the basement to several hundred meters above the reservoir. The abrupt termination of induced fractures against a fault can be explained in terms of geological structure, with major strike-slip faults acting as a barrier to fracture propagation.

From a drilling, completions, and production perspective, the well treatment objective

is to use hydraulic fracturing to open up the formation, inject proppant, and thereby increase the permeability of the reservoir. If minor fault reactivation is the dominant mechanism for reservoir enhancement in the Duvernay Formation, then an optimal completion program would orient the wells orthogonal to the predominant transtensional fault trends.

Oil maturation may be affected by basement faulting by increasing heat flow to local areas. Where localized high heat flow exists, condensate may be converted to dry gas, the final stage of oil maturation. There is insufficient data to make a direct correlation between basement faulting and the presence of dry gas, however this provides a plausible explanation for the unexpected high degree of heterogeneity.

The orientation of treatment wells with respect to pre-existing faults may be a key factor in causing large magnitude induced seismic events. In both areas studied here, large magnitude induced seismic events occurred when hydraulic fracture stimulation was performed in wellbores parallel to, and in close proximity to, basement-rooted faults (Eyre et al., 2019b,a; Eaton et al., 2018). This leads to multiple interactions between fluid injections and the faults. Depending on how the fault is locked, multiple stages of fracture stimulation may cause cumulative aseismic creep over a significant portion of the fault, resulting in sudden failure in the overlying unstable rock. A mitigation strategy may include orienting the well bores orthogonal (not parallel) to the basement faults, and by skipping the stages that intersect, or are in close proximity to, the fault.

The minor (transtensional) faulting and fracturing mapped in the Duvernay can change orientation over a relatively short distance, as shown in the seismic, structural mapping of the Swan Hills Formation in adjoining areas. Future drilling and well treatment could be optimized by taking into account pre-existing geological structures. The Bigstone North area has a preferred orientation for treatment wells in an east-west direction, orthogonal to the pre-existing fault and fracture lineations. This optimized well orientation would improve the treatment program by using the pre-existing fracture network and maximizing the stimulated reservoir volume. In contrast, a wellbore positioned parallel to a pre-existing fracture network would be ineffective in opening up the reservoir. The Swan Hills reef edge should also be taken into account, as it appears to be a significant barrier to fracture propagation. For the ToC2ME area, the preferred wellbore orientation is SE to NW, taking into account the preexisting Swan Hills structure in the area. This study has demonstrated that 3D seismic is a very effective tool for wellbore planning, and in addition to depth control, mapping vertical and strike-slip faulting provides useful information for treatment programs.

## **ACKNOWLEDGMENTS**

Sponsors of the Microseismic Industry Consortium and the sponsors of CREWES are thanked for their financial support of this study. The microseismic data were acquired using the BuriedArray method under license from Microseismic Inc. This work was supported by funding for the NSERC/Chevron Industrial Research Chair in Microseismic System Dynamics. TGS Canada is thanked for providing multi-component 3-D seismic data for this study, as well as an anonymous company for the use of the microseismic catalogue in the northern project area. We thank CGG for providing the Insight Earth Software, as well as the use of Geoview from Hampson Russell software. We also thank Seisware for interpretation and mapping software. This work was also funded by NSERC (Natural

Science and Engineering Research Council of Canada) through grants CRDPJ 461179-13, CRDPJ 474748-14, IRCPJ/485692-2014, and IRCSA 485691. We thank Divestco for providing digital LAS curves. We thank the SEG Earl D. and Reba C. Griffin Memorial Scholarship for their financial support in funding me for this research.

## REFERENCES

- Bjørlykke, K., 2018, Fluid flow in sedimentary basins: *Sedimentary Geology*, **86**, No. 1-2, 137–158.
- Duggan, J., Mountjoy, E., and Stasiuk, L., 2001, Fault-controlled dolomitization at swan hills simonette oil field (devonian), deep basin west-central alberta, canada: *Sedimentology*, **48**, No. 2, 301–323.
- Eaton, D., 2018, *Passive Seismic Monitoring of Induced Seismicity: Fundamental Principles and Application to Energy Technologies*: Cambridge University Press.
- Eaton, D., Igonin, N., Poulin, A., Weir, R., Zhang, H., Pellegrino, S., and Rodriguez, G., 2018, Induced seismicity characterization during hydraulic-fracture monitoring with a shallow-wellbore geophone array and broadband sensors: *Seismological Research Letters*, **89**, No. 5, 1641–1651.
- Eaton, D., Milkereit, B., Ross, G., Kanasewich, E., Geis, W., Edwards, D., Kelsch, L., and Varsek, J., 1995, Lithoprobe basin-scale seismic profiling in central alberta: Influence of basement on the sedimentary cover: *Bulletin of Canadian Petroleum Geology*, **43**, No. 1, 65–77.
- Eyre, T., Eaton, D., Garagash, D., Zecevic, M., Venieri, M., Weir, R., and Lawton, D., 2019a, The role of aseismic slip in hydraulic fracturing–induced seismicity: *Science advances*, **5**, No. 8, eaav7172.
- Eyre, T., Eaton, D., Zecevic, M., D’Amico, D., and Kolos, D., 2019b, Microseismicity reveals fault activation before mw 4.1 hydraulic-fracturing induced earthquake: *Geophysical Journal International*, **218**, No. 1, 534–546.
- Fossen, F., and Tikoff, B., 1998, Extended models of transpression and transtension, and application to tectonic settings: *Geological Society, London, Special Publications*, **135**, 15–33.
- Knapp, L., McMillan, J., and Harris, N., 2017, A depositional model for organic-rich duvernay formation mudstones: *Sedimentary Geology*, **347**, 160–182.
- Li, Z., Chi, G., and Bethune, K., 2016, The effects of basement faults on thermal convection and implications for the formation of unconformity-related uranium deposits in the athabasca basin, canada: *Geofluids*, **16**, No. 4, 729–751.
- Poulin, A., Weir, R., Eaton, D., Igonin, N., Chen, Y., Lines, L., and Lawton, D., 2019, Focal-time analysis: A new method for stratigraphic depth control of microseismicity and induced seismic events: *Geophysics*, **84**, No. 6, KS173–KS182.
- Preston, A., Garner, G., Beavis, K., Sadiq, O., and Stricker, S., 2016, *Duvernay reserves and resources report: A comprehensive analysis of alberta’s foremost liquids-rich shale resource*: Alberta Energy Regulator, Calgary, 83.
- Shen, L., Schmit, D., and K., H., 2019, Quantitative constraints to the complete state of stress from the combined borehole and focal mechanism inversions: Fox creek, alberta: *Alberta Tectonophysics*, **764**, 110–123.
- Switzer, S., Holland, W., Christie, D., Graf, G., Hedinger, A., McAuley, R., Wierzbicki, R., Packard, J., Mossop, G., and Shetsen, I., 1994, Devonian woodbend-winterburn strata of the western canada sedimentary basin: *Geological Atlas of the Western Canada Sedimentary Basin*: Canadian Society of Petroleum Geologists and Alberta Research Council, 165–202.
- Tissot, B., and Welte, D., 1984, *Petroleum formation and occurrence*, springer-verlag: Berlin, Germany.

- Wang, R., Gu, Y., Schultz, R., Zhang, M., and Kim, A., 2017, Source characteristics and geological implications of the january 2016 induced earthquake swarm near crooked lake, alberta: *Geophysical Journal International*, **210**, 979–988.
- Weir, R., Eaton, D., Lines, L., Lawton, D., and Ekpo, E., 2018, Inversion and interpretation of seismic-derived rock properties in the duvernay play: *Interpretation*, **6**, No. 2, SE1–SE14.
- Weir, R., Lawton, D., Lines, L., Eyre, T., and Eaton, D., 2019, Application of structural interpretation and simultaneous inversion to reservoir characterization of the duvernay formation, fox creek, alberta, canada: *The Leading Edge*, **38**, No. 2, 151–160.
- Zhang, H., Eaton, D., Rodriguez, G., and Jia, S., 2019, Source-mechanism analysis and stress inversion for hydraulic-fracturing-induced event sequences near fox creek, alberta: *Bulletin of the Seismological Society of America*, **109**, No. 2, 636–651.